GEOLOGICAL SURVEY OF FINLAND
Applied Geophysics
Espoo

GTK Open File Work Report
February 8, 2019

KOSE – Koillismaa Seismic Exploration survey: Acquisition, processing and interpretation

Gardar Gislason, Suvi Heinonen, Heikki Salmirinne, Jukka Konnunaho, Tuomo Karinen

Geologian tutkimuskeskus | Geologiska forskningscentralen | Geological Survey of Finland
Espoo • Kokkola • Kuopio • Loppi • Outokumpu • Rovaniemi
www.gtk.fi • Puh./Tel. +358 29 503 0000 • Y-tunnus / FO-nummer / Business ID: 0244680-7

GEOLOGICAL SURVEY OF FINLAND **DOCUMENTATION PAGE**

February 8, 2019

Authors
Gislason, Gardar
Heinonen, Suvi
Karinen, Tuomo
Konnunaho, Jukka
Salmirinne, Heikki

Type of report
GTK Open File Work Report

Comission by
GTK

Title of report
KOSE – Koillismaa Seismic Exploration survey: Acquisition, processing and interpretation

Abstract
GTK has carried out a seismic survey in the Koillismaa area, located in the municipality of Kuusamo, north-eastern Finland. The Koillismaa Seismic Exploration (KOSE) survey was motivated by a 5 km wide and 50 km long gravity anomaly between the Koillismaa and Näränkävaara intrusions. This gravity anomaly is thought to be an Archean greenstone belt or a feeder channel for the Koillismaa layered intrusion. Previous interpretations of the Bouguer gravity anomalies suggest a dyke-like intrusion of about 2.5 – 4 km width and a depth to the top part around 1 – 2 km. The KOSE survey was aimed to estimate the depth and dip of this unknown body.

The survey was a part of a collaboration project between GTK and Oulu University and was carried out using 90 wireless receivers owned by Oulu University. The resulting seismic sections span 8.1 km length and reveal a strong reflector at 3.3 km depth and a weaker one at 1.3 km depth. This suggests a top part of the intrusion to be ~1.3 km deep and a bottom part at 3.3 km, which would make the intrusion 2 km thick.

Keywords
Koillismaa, Kuusamo, Näränkävaara, seismic exploration, Ni-Cu-PGE, mineral potential

Geographical area
Koillismaa

Map sheet
4521

Other information

Report serial
GTK Open File Work Report

Archive code
101/2018

Total pages	Language	Price	Confidentiality
33 pages	English	-	Public

February 8, 2019

Unit and section Applied Geophysics	Project code 50402–2006621
Siganture/name  Heikki Forss	Signature/name  Gardar Gislason

Contents

Documentation page

ABBREVIATIONS

1C	One/single component sensor (geophone)
3C	Three/triple component sensor (accelerometer)
CDP	Common Depth Point.
Data logger	Recording instrument that records data measured with a sensor
Profile	The measurement line with all receivers included.
Receiver	Includes both sensor and data logger as one unit.
Sensor	Geophone (1C) or a MEMS accelerometer (3C)
Spread	The measurement line with all *active* receivers included (Figure 1.6).
TWT time	Two-Way-Travel time. The time it takes for a wave to travel down and upwards from a reflector.

1 INTRODUCTION

The Koillismaa-Näränkävaara Complex (Fig. 1.1) is a part of the ca. 2440 Ma Tornio-Näränkävaara Intrusion belt running across Finland from the Finnish-Swedish border to the Finnish-Russian border. The emplacement of these intrusions is a part of a large 2450-2500 Ma plume-related rifting event (Alapieti 2005). This event belongs to a global episode of igneous activity in the beginning of the Proterozoic that produced several layered intrusions and mafic dyke swarms on other cratons as well and was, at least in Fennoscandia, related to the initial breakup of an Archaean craton (Alapieti & Lahtinen 2002, Iljina & Hanski 2005).

In 2018, Geological Survey of Finland (GTK) and University of Oulu (UO) conducted a seismic survey to study a deep seated gravity and magnetic anomaly located between the Koillismaa and Näränkävaara intrusions (Fig. 1.1). There have been many speculations on the source of these prominent gravity and magnetic anomalies, and the main aim of the seismic survey was to estimate the depth and dip of the source of the anomalies. The seismic field work is part of the GTK and UO co-operation, where seismic methods are tested in different pilot study areas including mineral exploration, ground water and urban targets.

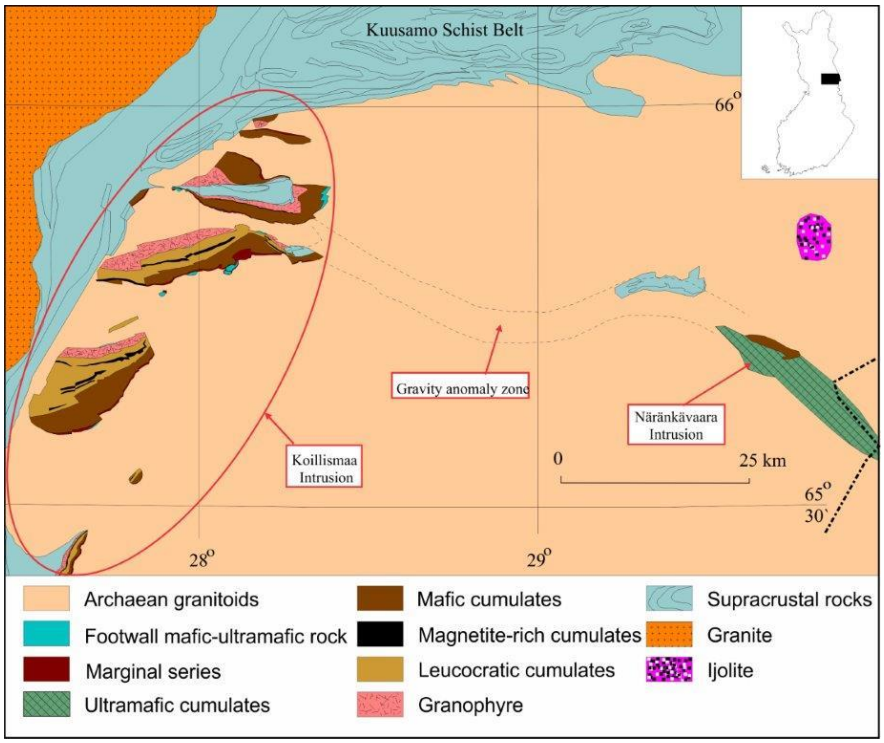

Figure 1.1: The gravity anomaly is located between the 2.45 Ga Koillismaa Layered Intrusion Complex (KLIC) and the Näränkävaara ultramafic body (Karinen 2010)

We acquired an 8.5 km long seismic profile across a 50 km long and 5 km wide magnetic and gravity anomaly (Fig. 1.2). Previous interpretations of the Bouguer anomaly suggest a dyke intrusion of about 2.5 – 4 km width and a depth to the top part around 1 – 2 km, as shown in

Figure 1.3 (Salmirinne & Iljina, 2003). The KOSE survey was aimed to estimate the depth and dip of this unknown body. As usual for the seismic survey, the profile line had to be planned to follow an existing road which limited the possible locations to acquire data.

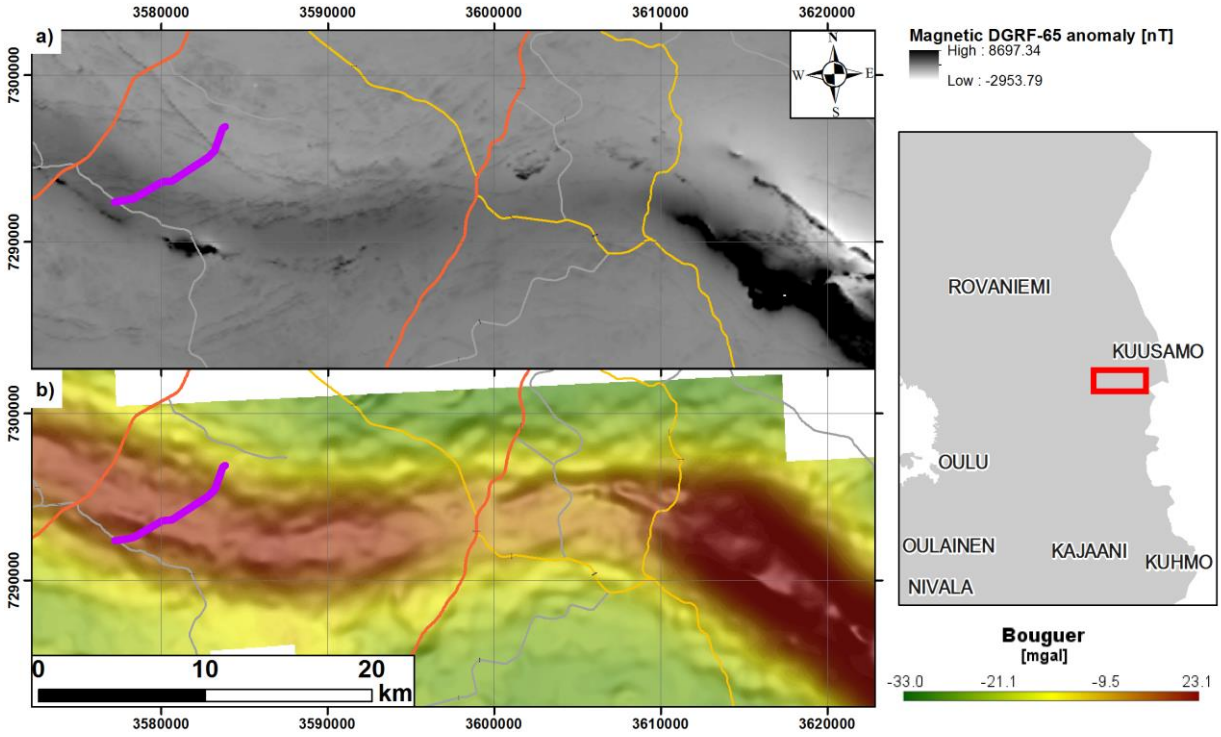

Figure 1.2: Magnetic anomaly (a) and Bouguer gravity anomaly (b). Main roads are included on the map (red, yellow and gray) and the acquired seismic profile is in purple. The maps are in KKJ3 coordinates. Smaller roads are shown in Figure 2.3.

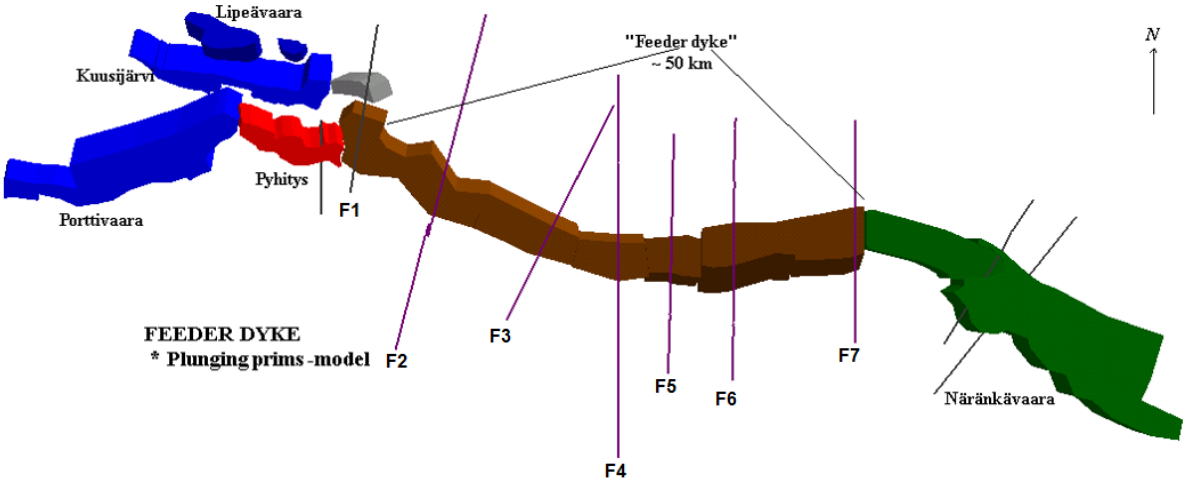

Figure 1.3: Bouguer gravity model suggest a 50 km long and 2.5-5 km wide feeder dyke (brown) between the Koillismaa intrusions (blue and red) and the Näränkävaara ultramafic body (green). Seven gravity profiles are shown in the figure from F1-F7. The seismic profile from this survey is near gravity profile F3. Figure by Salmirinne & Iljina, 2003.

2 DATA ACQUISITION

2.1 Instrumentation

Figure 2.1: The 1C geophone and data logger (left) and the 3C accelerometer and data logger (right).

The seismic receiver system used in this survey is owned by Oulu University. The recording equipment consisted of 35 three component (Figure 2.1, right) and 55 one component (Figure

2.1, left) sensors and data loggers. The three component sensors are MEMS accelerometers, which means it is a digital sensor, while the one component sensors are geophones which are analog (Table 2.1).

Table 2.1: The equipment (sensor and data logger) names.

	3 component accelerometer	**1 component geophone**
Sensor	DSU3SA	SG-10
Data logger	RAU eX-D	RAU eX

Figure 2.2: GTK's newly purchased BoomBox.

We used dynamite as a seismic source. For accurate GPS time of each shot (or explosion), we used BoomBox 3 by Seismic Source Ltd – a newly purchased trigger system of GTK. This system gives the GPS time with microsecond accuracy. In the field, the Boom Box connects via Wi-Fi to a field laptop, tablet or a phone. During this survey, a phone was used to write down the shot ID and file ID of each shot. These data are saved in the BoomBox together with the GPS time stamps and can be later extracted either via a Wi-Fi connection or a direct connection to a laptop.

The GPS positions of receiver and shot locations were measured by GTK personnel.

2.2 Field work

In mid-March, 2018, Kenttärata road (Figure 2.3) was ploughed to allow access to it from the south side. As the road was built during the war years 1939-1944, the profile needed to be measured to look for magnetic anomalies that could be Unexploded Ordnance (UXO). The road area was investigated using an Overhauser magnetometer and a GEM-2 mini-slingram, and anomalous locations were marked on a survey map.

For the explosive sources, a total of 197 holes were drilled along the profile. The drill hole depth was approximately 2 m, and a plastic pipe with a cap was installed in each of the holes.

Holes were not drilled nearby the anomalous features revealed by the UXO investigations (see appendix A). Drill hole spacing was 40 m, allowing for offset along the profile if there was a measured anomaly nearby. Holes were drilled on the western side of the road, while the receivers were placed on the eastern part of the road (~3 m offset).

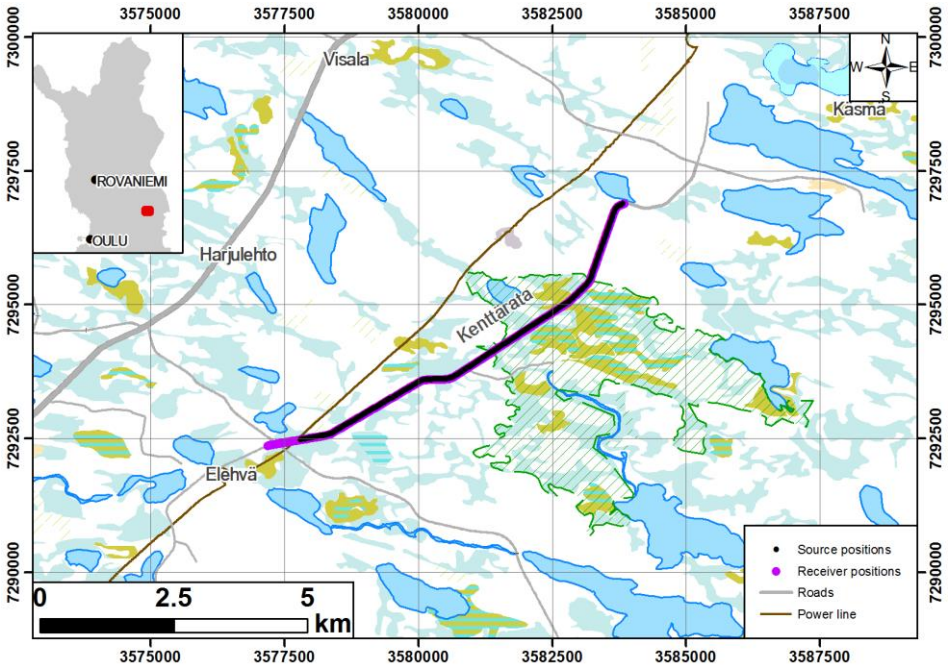

Figure 2.3: The survey line on Kenttärata road with receiver (purple) and source (black) positions. The map is in KKJ3 coordinates.

The field, data acquisition started on 16. April, 2018 and ended on 25. April, 2018. The first and last days were reserved for travelling to the survey site, equipment check and reconnaissance. As the field work was carried out in the start of the melting season, there was still a thick (> 1m) snow coverage. Field assistants surveyed the area on Friday, 13. April, 2018 and concluded that an excavator would be needed to properly plant the sensors into the ground. Using a measurement tape, they marked each receiver location in the snow. Afterwards an excavator went along the road and dug on the side of the road through the snow cover (Figure 2.4). Geophones need to be planted on the ground in order to enable good coupling and thus removal of snow coverage prior to the actual data acquisition made geophone deployment faster.

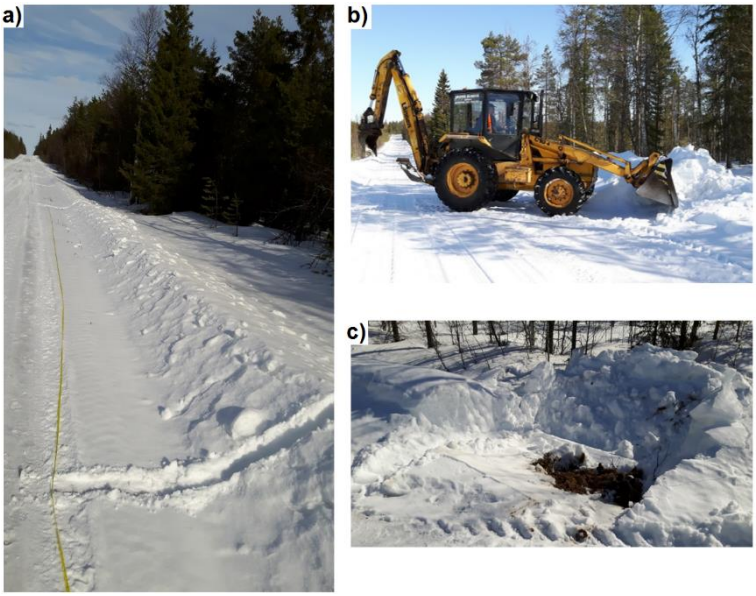

Figure 2.4 The receiver locations were marked (a) for the excavator (b). The excavator dug through the snow cover to the ground (c).

Table 2.2 Survey parameters.

Receiver parameters		**Source parameters**	
Receiver spacing	20 m	Source spacing	40 m
Active channels	90	Total source points	197
Spread length	1800 m	Depth of explosion	~2 m
Profile length	8500 m	Charge size	120-240 g
Sampling interval	1 ms		

The survey parameters are shown in Table 2.2. The source points were drilled to 2 m depth, unless there were obstacles, such as stones, in the way. In shallow holes smaller charge sizes (120 g) were used for explosions. A total of 90 wireless receivers were planted with 20 m spacing forming an 1800 m long spread. We used sampling interval of 1 ms (1 kHz).

The first receiver spread was set up on the morning of 17. April, 2018, on the northern end of the line. Using small amount of dynamite we did test shots on the northern edge of the spread for QC purposes. After determining that the spread was set up right, we started shooting and recording.

Figure 2.5 The receivers were split into 5 groups of 18 with semi-even distribution of 1C (yellow triangles) and 3C (yellow triangles with a green outline) components.

As we had 35 three component receivers and 55 one component sensors, we split the total 90 receivers into a group of 5. Each group had 18 receivers with a semi-even distribution of 1C and 3C sensors (Figure 2.5). The five groups together made a spread (Figure 2.6) of the 90 active receivers.

Figure 2.6 A receiver spread consisted of 90 receivers (5 groups).

After laying out the first spread, the source locations at the first 3 receiver groups (54 receivers -> 27 source points) were exploded (Figure 2.7). Next, the first receiver group (18 receivers) was "rolled" to the other end of the spread. This is called a roll-on split-spread configuration, and is based on the principle of shooting the explosives in the middle of each spread for best offset coverage. After finishing "rolling", the source locations at the next receiver group were exploded (9 source points). This was then continued to the end of the whole profile. The location of each shot and receiver point was measured with GPS.

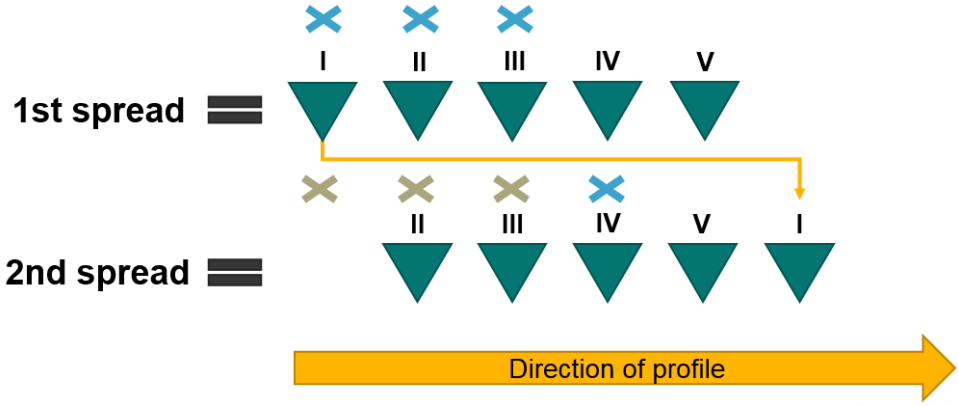

Figure 2.7 After exploding dynamite until the 3rd receiver group (blue crosses of the 1st spread), the first group was rolled to the front of the line. After that, dynamite was exploded to the next receiver group (blue cross of the 2nd spread).

After each field day, we brought the data loggers to the field base, but left the sensors in the field. This way we could save the data acquired during the day the same evening for QC purposes and to ease processing at a later stage. The morning after, we only had to plug in the data loggers at each receiver location.

There was a large power line at the southern end of the road preventing continuation of the shooting explosives further south. This is the reason for the receiver line reaching further than the source line as shown in Figure 2.3.

3 DATA PROCESSING

3.1 Preparation

After each field working day, the data were extracted from the data loggers and checked. The geometry of the survey layout was created after each field working day with the measured GPS coordinates of the receiver and shot locations.

We used TM35 coordinate system for the KOSE seismic survey. The coordinates were later truncated to fit into the GLOBE Claritas coordinate system with the following equations:

$$X = X_{TM35} - 580000 \quad , \qquad Y = Y_{TM35} - 7290000 \qquad \textbf{[3.1]}$$

The data were downloaded from the data loggers in a SEG-D format. This was imported to GLOBE Claritas processing software using an .sdhd file, specifying at which byte specific header information is stored. The most important one is the header which contained information of which component each trace belongs to. We defined the SEGY header "USE" for this purpose. Each trace would then have USE=1 or 2 or 3, depending on if it was vertical (1) or horizontal (2 or 3) components.

Table 3.1 Process list of importSEGD_wGEOM.job

Process	Details
Read all SEG-D to SEGY	Sdhd file: "151210.sdhd"
QC of traces	Remove channels 22 and 23 of SHOT ID 182.
Remove H component	Keep only USE=1 traces
Renumber channels	Renumber from 1 to 90 per SHOT ID
Add geometry	Add geometry to headers: "KoSe_wShotDepths_ CDP.geom"
Write .hdf5 file	"KoSe_VerticalCompData_ Full_wGEOM.hdf5"

The process of acquiring the raw vertical component data is shown in Table 3.1. The processing done here includes only the vertical component traces (USE=1). The total number of traces acquired were 160 (55*1 + 35*3), 90 of which are vertical component.

In general there were no technical errors in the data. However, for SHOTID 182 a 3C station had failed causing SHOTID 182 to have 2 extra vertical component traces. The data of the failed receiver was stored in the channel numbers 21, 22 and 23 (original channel number), but was erroneously marked as three 1C traces from the SEG-D file. A simple solution to this was to delete channels 22 and 23.

3.2 Processing

Processing of the data was done with GLOBE Claritas software and the processing flow, including .job-files utilized in Claritas, are presented in this chapter.

A first step in the processing was to create a brute stack, which essentially stacks the acquired data with a constant velocity of 6000 m/s (Figure 3.1). The arrow on the figure indicates a very clear reflector that is visible even in the noisy pre-processed stack. The reflector is at ~1.1 s TWT (Two Way Travel) time. This means that, since we use a 6000 m/s constant velocity, the reflector would have a depth of 3300 m. The first visualization of the subsurface reflectivity was done in *01_brute_stack.job* processing flow.

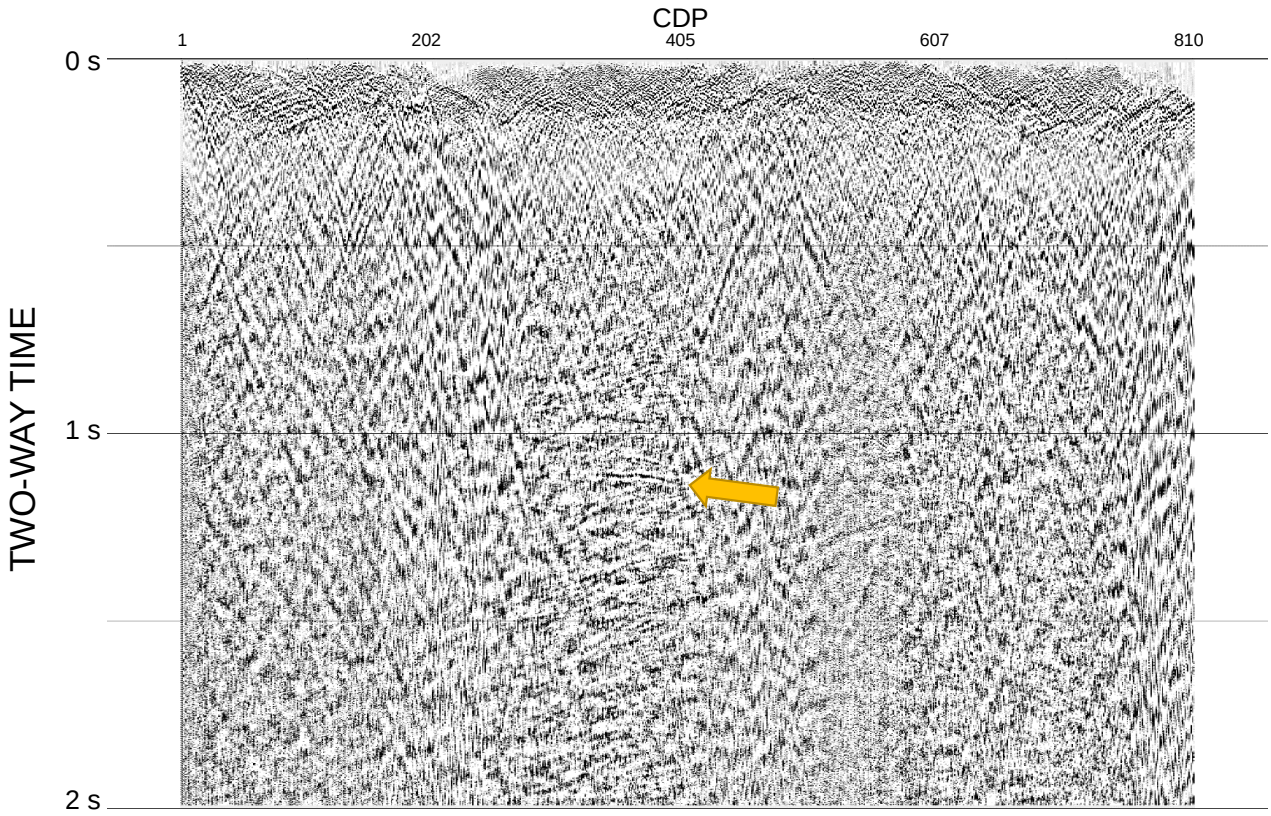

Figure 3.1 Brute stack with 6000 m/s NMO and a 500 ms AGC applied.

The raw data (Figure 3.2a) show substantial delays in the first arrivals (seismic waves refracted from the interface between overburden and bedrock). With 20 m receiver spacing, the time delays of the first arrivals indicate highly varying thickness and velocity structures in the overburden. As previously mentioned, the survey was carried out in the melting season, and water saturated or frozen ground can also be a contributing factor to the nonlinear arrival times. The time delays caused by the overburden are eliminated with refraction static corrections. This requires the picking of the first arrival of each trace in each shot, making total of 17730 picks. After the first break picking, a subsurface velocity variations were modeled. In this process, travel times of the refracted seismic waves are calculated based on an initial model of the subsurface. The calculated travel times are then compared to the picked ones, and mode iteratively modified to improve the fit until difference between picked and calculated fist arrivals is minimized. Both layer thickness and velocity within the layer can be modified during the iteration process. Figure 3.2b shows one shot gather with the statics applied. When comparing Figure 3.2a and b, it is clear that the static corrections are important processing step correcting data acquired by different receiver to the same reference datum. A refraction statics QC job was performed in 02a, 02b and 02c .job files to check that the first break picks were right and that the data were improved. The refraction statics resulted in a velocity model of the shallow subsurface which is shown in the Figure 3.3.

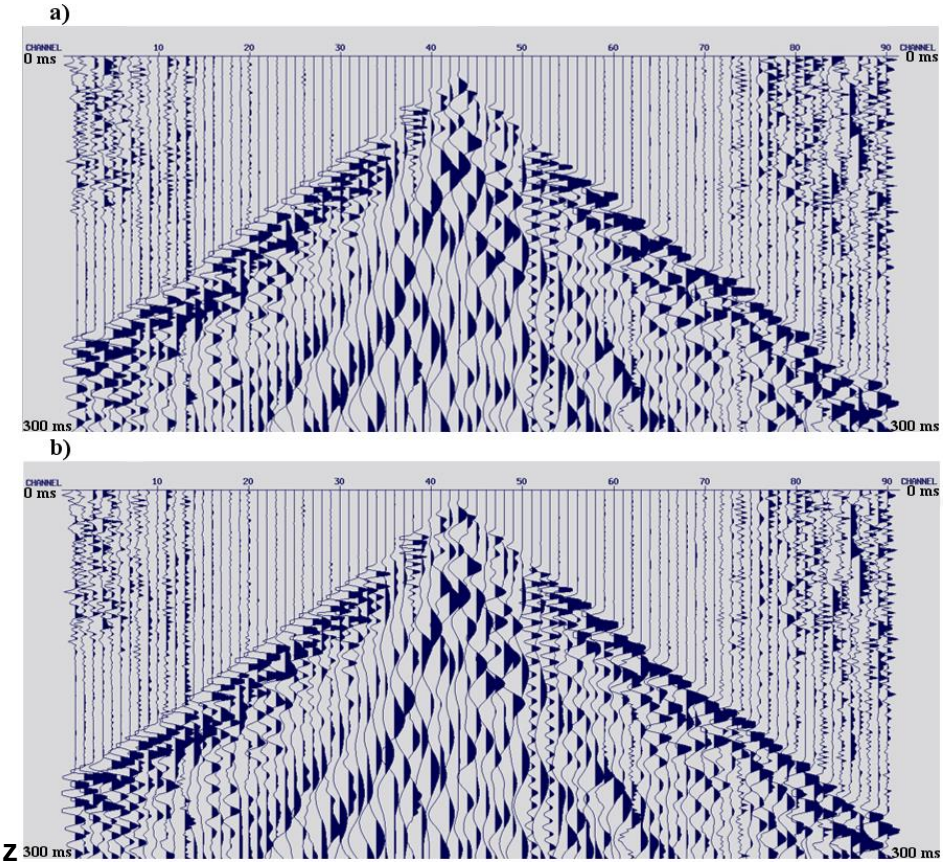

Figure 3.2 Raw "wiggle" plot of shot ID 25 with a) AGC applied and b) AGC and statics applied. The data shown are from 0 – 300 ms TWT.

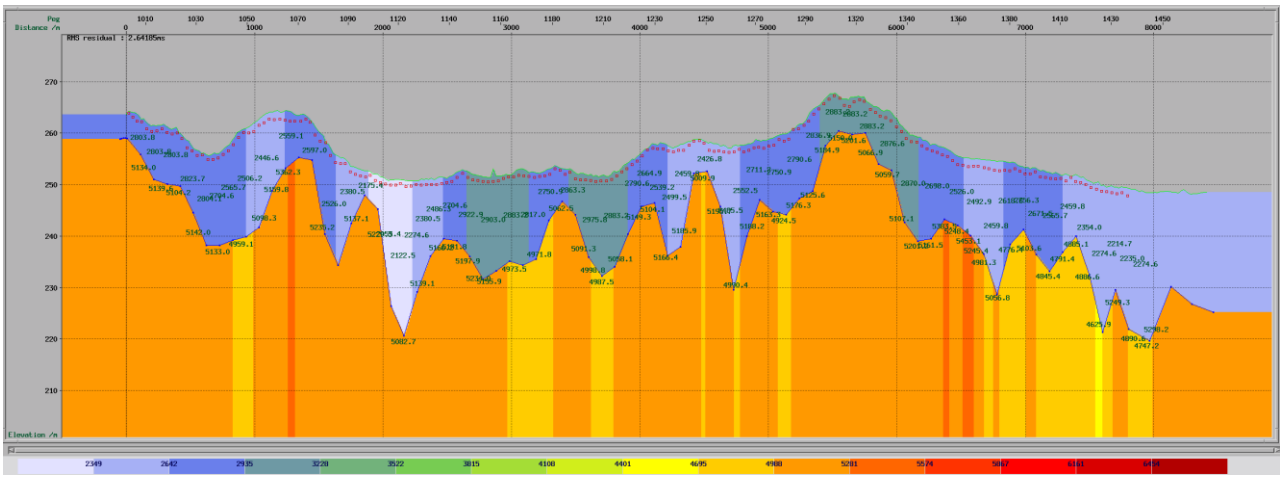

Figure 3.3 The subsurface velocity beneath the 8.1 km long seismic profile. The color scale is from 2350 m/s (light blue) to 4700 m/s (orange) and to 6500 m /s (red).

Because of the sparse receiver spacing of the survey, the highest frequency we can sample is limited and high frequency signals might be spatially aliased. Figure 3.4 shows the F-K domain of shot IDs 3 and 25. On shot ID 3, the energy looks normal until the right edge (K=1), where it wraps around to the left edge (K=-1). According to the spatial aliasing formula (equation [3.2]), the highest frequency we can correctly sample depends on the subsurface velocity (v), receiver spacing (Δx) and the dip (θ). The aliasing in our dataset starts at ~135 Hz, which we can plug into the equation along with the 6000 m/s velocity and the 20 m receiver spacing. This results in: $\theta_{max} \approx 34°$, which is the maximum dip that we can correctly map onto a seismic section.

$$f_{\max} = \frac{v}{4\Delta x \sin\theta} \qquad \textbf{[3.2]}$$

To unwrap the aliasing, we created synthetic traces between the existing ones, essentially halving the receiver spacing (from 20 m to 10 m). Then to de-alias, an F-K mute is applied at |K|>0.5. Afterwards the synthetic traces are removed. Figure 3.5 shows the same shot IDs with this anti-aliasing applied. The wrapped around energy has been muted while still keeping the non-aliased energy.

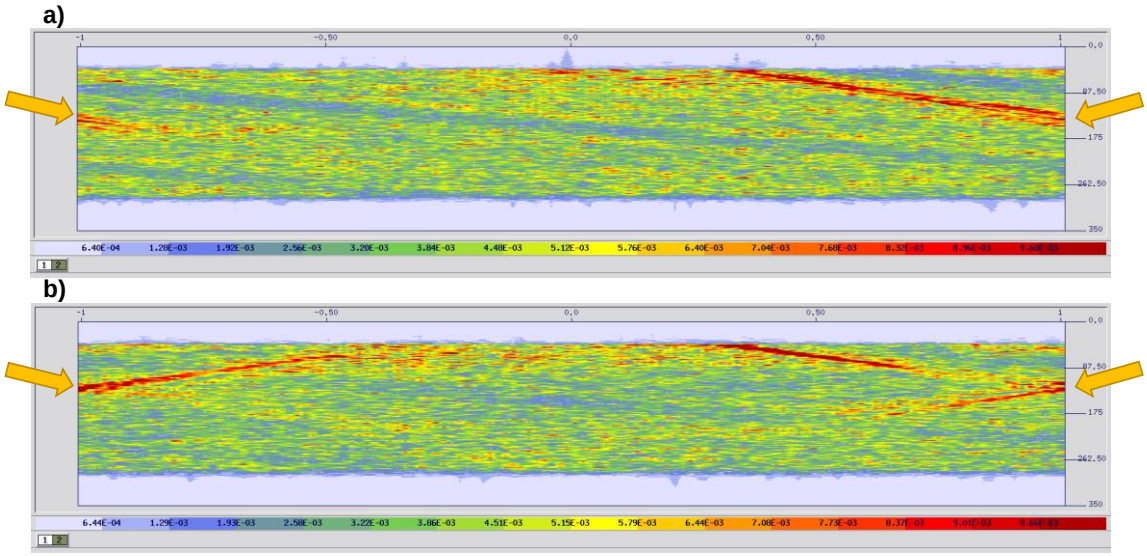

Figure 3.4 F-K domain plot of a) shot ID 3 and b) shot ID 25. On the edges of both the plots, the energy wraps around and starts on the other edge. This starts at ~135 Hz. File name: 04a_prestack_proc_fxdecon_ BP40-45-275-300.shots

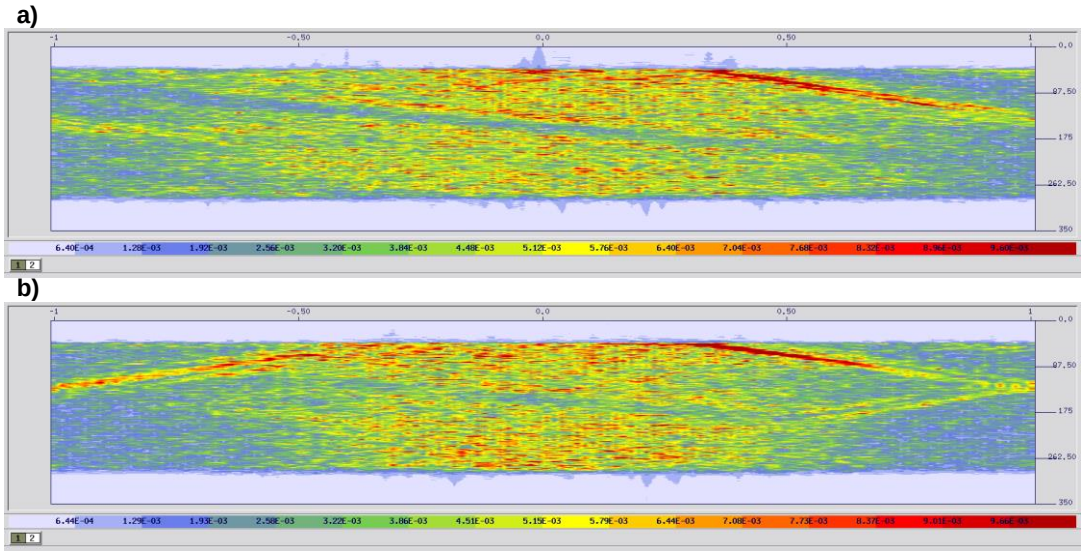

Figure 3.5 F-K domain of de-aliased a) shot ID 3 and b) shot ID 25. The wrapped around energy has been muted while keeping the non-aliased energy.
File name: 04a_prestack_proc_aliasFIX_fxdecon_BP40-45-275-300.shots

Figure 3.6a shows if, instead of this anti-aliasing technique, we would cut the frequency at 135 Hz, so that there would be no aliasing. This leaves us with much lower frequency to image the reflection indicated with a yellow arrow. With no de-aliasing (Figure 3.6b), but keeping the same processing flow as in Table 3.2, the reflection is much clearer. With the de-aliasing from Table 3.2 (Figure 3.6c), the shot gather shows very similar results to Figure 3.6b. However, as Figure 3.4 shows, the data is spatially aliased and thus we decided to keep the anti-aliasing filter as a pre-caution to not pick aliased dip reflectors.

A noise QC job was performed in 03a, 03b and 03c, using the AREAL module of Claritas, to remove too high amplitude traces. This did not improve the results significantly and was thus not used.

The pre-stack processing job file description is shown in Table 3.2. The offset was set to absolute offset for future refraction mute. The anti-aliasing routine is shown in the table and includes doubling the trace number per shot, trace amplitude mixing and FK-mute of aliased energy. The .bmu mute file was created with the muting application of Claritas (Miscellaneous tab). The file contains a |K|>0.5 mute with 30 vertical and 6 horizontal average cosine smooth to minimize artifacts from sudden cut of the mute.

The band pass filter was selected after multiple tests as 40-45-275-300 Hz. At the top 500 ms, 75-80-275-300 Hz proved to be a better filter because it is efficiently suppressing the low frequency noise caused by ground roll. However, this higher frequency BP filter was not used as there were no observable reflections in the top 500 ms and deeper reflections are most apparent with lower frequencies. Figure 3.7 shows the processed plot with the frequencies

isolated. Although the strong reflector's amplitude is the strongest at 50 – 100 Hz, there is still some energy in the higher frequencies that can be useful to detect the low amplitude reflectors.

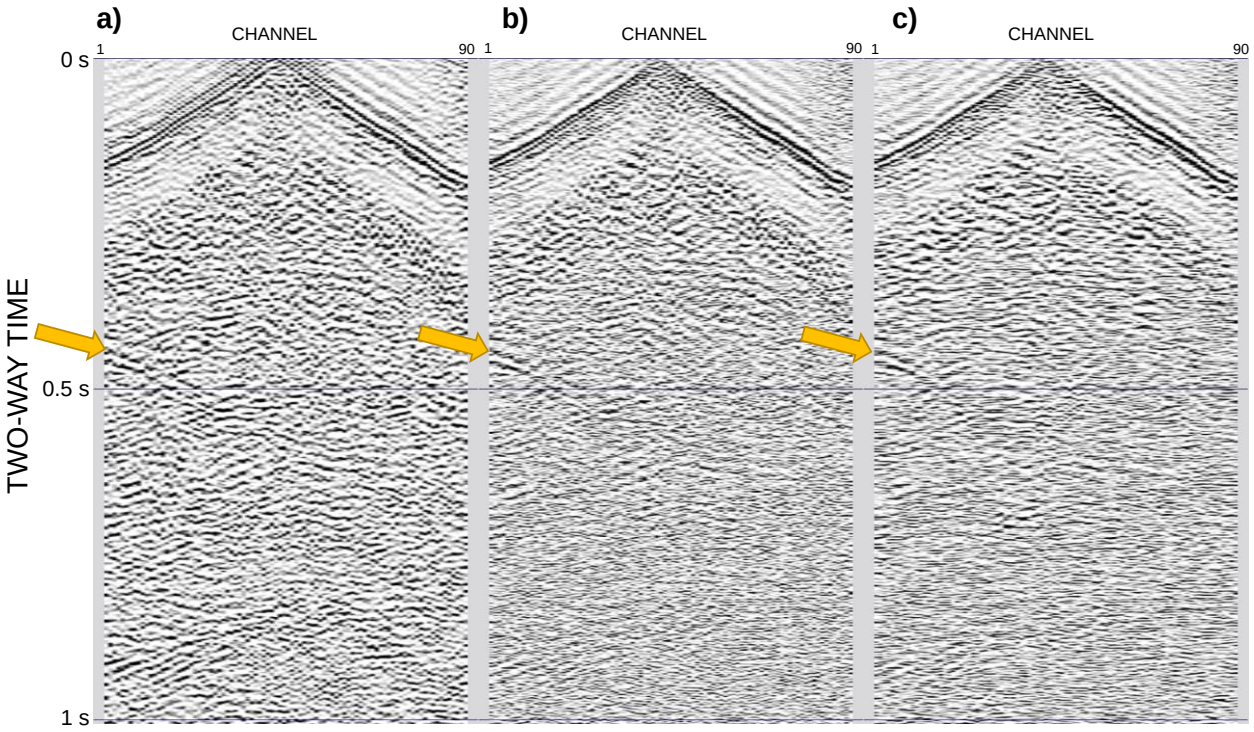

Figure 3.6 The processed shot gathers of shot ID 25 with a) no de-aliasing and BP40-45-120-135 Hz, b) no de-aliasing, and c) with de-aliasing. All other processing steps are from Table 3.2.

Spiking deconvolution was used to convert the wavelets to minimum phase and thus increase coherency. The airwave was attenuated utilizing velocity 330 m/s. Afterwards an FX-deconvolution was used as a coherency filter between the traces to increase reflection amplitudes. The 3000 m/s median filter was implemented to get rid of the noisy, dipping arrivals that were not reflections but S-wave first arrivals. After deconvolution, airwave and S-wave attenuation, the same BP filter was applied as before along with an AGC using 200 ms filter length.

Table 3.2 Process list of 04a_fk_aliasing_fix.job

Process	Details
Read SEGY	"KoSe_VerticalCompData_Full_wGEOM.hdf5"
HDRMATH	Offset=abs(offset)
STATIC	Static corrections with "ref1_pass3_total.shf", 6000 m/s replacement velocity and 260 m fixed datum.
AGC	200 ms
Anti-Alias: MISSING	Add synthetic traces
Anti-Alias: RUNMIX	Weighted mix of 3 adjacent traces.
Anti-Alias: FKMUTE	Mute in the F-K domain with "FKMUTE_0.5Koutside_30V_6H_cosineAverage.bmu"
Anti-Alias: TREMOVE	Remove synthetic traces
Anti-Alias: RENUMBER	Renumber the original traces.
FDFILT	BP 40-45-275-300 Hz
DECONW	Spiking deconvolution
AIRWAVE	330 m/s airwave attenuation
FXDECON	Pre-stack coherency filter
MEDIANH	3000 m/s median filter
FDFILT	BP 40-45-275-300 Hz
AGC	200 ms
Write .hdf5 file	"04a_prestack_proc_aliasFIX_fxdecon_BP40-45-275-300.shots"

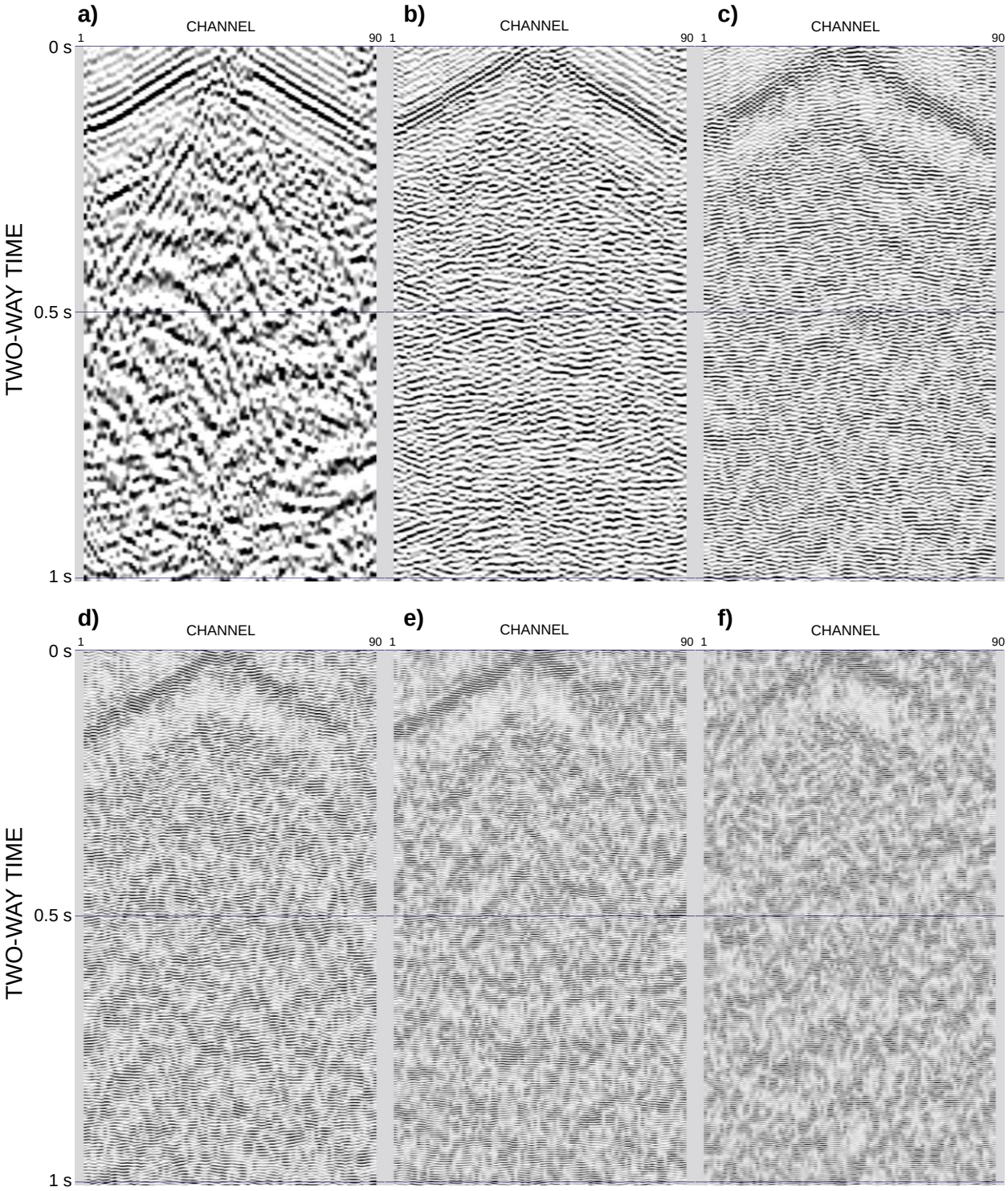

Figure 3.7 Processed shot gathers of shot ID 25 from Table 3.2 but with band pass filter; a) 10 – 50 Hz, b) 50 – 100 Hz, c) 100 – 150 Hz, d) 150 – 200 Hz, e) 200 – 250 Hz, f) 250 – 300 Hz.

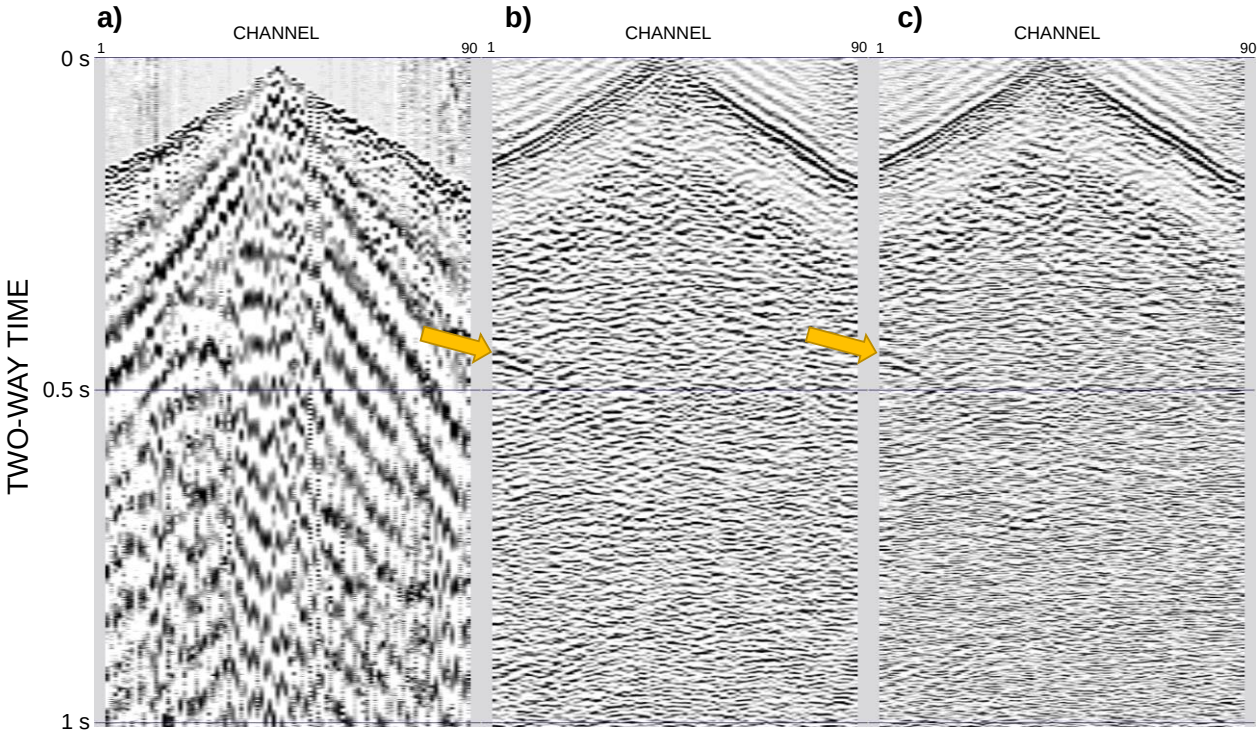

Figure 3.8 a) Raw and b) processed shot gather with 40-45-175-200 Hz BP filter and c) processed shot gather with 40-45-275-300 Hz BP filter for shot ID 25.

A muting QC analysis was done in job 05, to see if an angle-mute or a picked refraction mute should be used. A picked refraction mute was selected and is found in the file *"refr_mute.smu"*.

Figure 3.8 shows the side-by-side comparison of the data before and after the pre-stack process flow. In Figure 3.8b, a 40-45-175-200 Hz band pass filter was used instead of the one from 40-45-275-300 Hz band pass filter from Table 3.2. Although the lower frequency band pass filter images the reflector, the higher frequencies give a crisper image and were thus preferred. A prominent reflector is seen in the left edge of the processed shot gathers and is indicated with arrows. Unprocessed data is dominated by low frequency noise that has been efficiently suppressed by the processing.

3.3 Stack and migration

In job 06, a velocity analysis was made. Due to the low amount of reflectors in the top 1000 ms, it became difficult to pick velocities and we decided on a constant velocity of 6000 m/s.

Table 3.3 Process list of 07a_stack_nmo.job

Process	Details
Read .hdf5 file	"04a_prestack_proc_aliasFIX_fx decon_BP40-45-275-300.shots"
SMUTE	Refraction top mute with: ref_mute.smu
NMO	6000 m/s constant velocity.
FDFILT	BP 40-45-275-300 Hz
AGC	200 ms
RUNMIX	Weighted mix of 3 adjacent traces.
STACK	SQRT Normalized stack.
BALANCE	Full trace balance
Write .hdf5 file	"07a_6000CVS_40-45-275-300_aliasFIX.stack"

Stacking of the pre-stack processed shot gather was made with job 07a. The details of the processing flow is shown in Table 3.3. AGC was used for consistent energy distribution, especially for the top 500 ms as without a 200 ms window, an amplitude shadow is formed. As previously mentioned, a constant velocity of 6000 m/s was used for NMO followed by the same band pass filter as before for consistency. A weighted mix of 3 adjacent traces was made for reflector coherency. Then the data were stacked and amplitude balanced.

The stack is seen in Figure 3.6 along with arrows indicating the possible reflectors. There are clearly more reflectors visible, compared to the brute stack from Figure 3.1.

Normally, after stacking, the next step is to do surface-consistent residual statics. Jobs 08a, 08b and 08c perform this, but because of the low amount of reflectors, the results did not improve and thus no residual statics are used in the production of the final seismic stack.

The data were migrated using a standard, computationally cheap and simple STOLT migration that is often used for hardrock seismic data where subsurface velocity variations are not well known. The processing flow is described in Table 3.4. Essentially, it included a zeromute to store the top mute; a padding on both side to allow for migration out of the line; the migration itself and then the removal of the padded traces. The same band pass filter as before was applied to remove the low frequencies that were introduced during the migration. To create a .segy file from these .hdf5 files, job 13 was used. The job description is shown in Table 3.5. Figure 3.7 shows the stack after the processing flows from 3.4 and 3.5, including time-to-depth conversion.

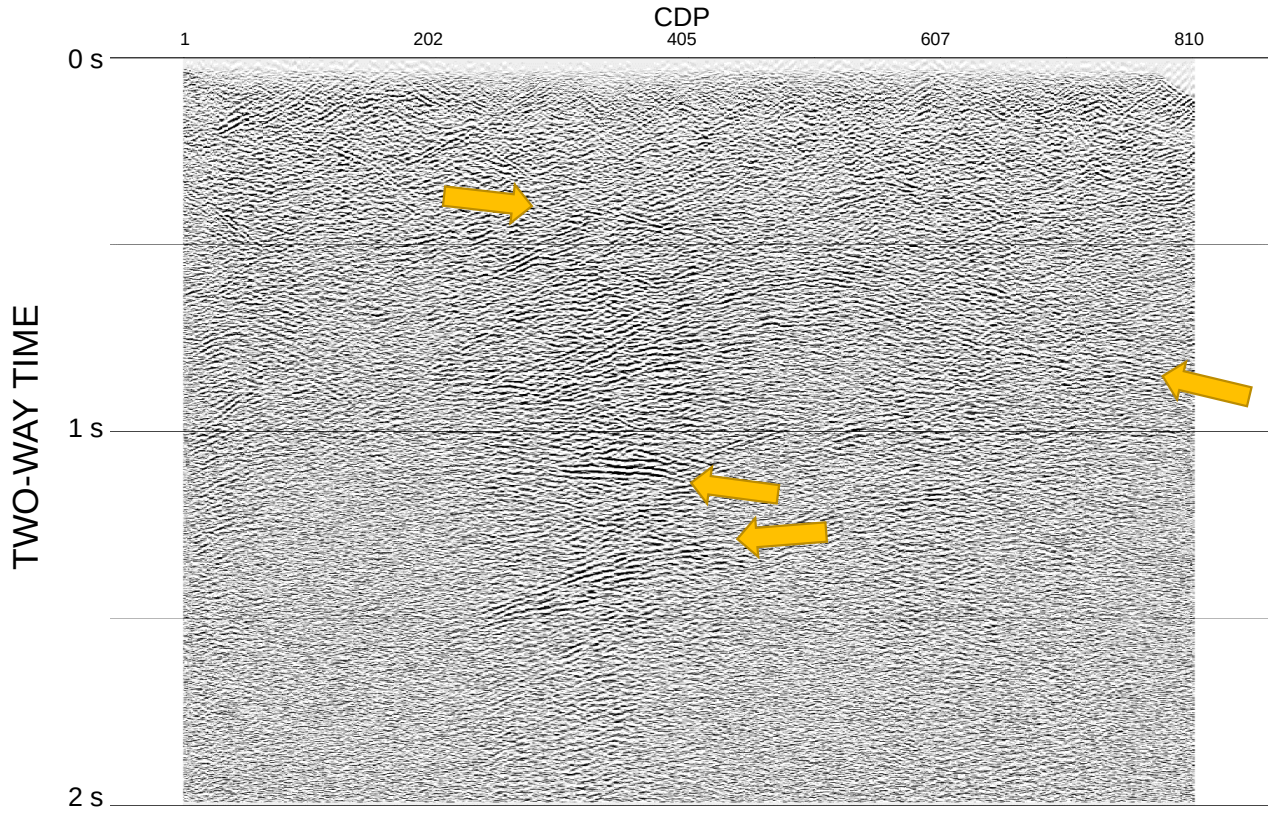

Figure 3.9 The full stack after the processing flow from Table 3.3.

Table 3.4 Process list of 07b_migrate_stacks.job

Process	Details
Read .hdf5 file	"07a_6000CVS_40-45-275-300_aliasFIX.stack"
Migration: ZEROMUTE	Store delay header which contains the top mute.
Migration: PAD	Pad with 100 traces to each end
Migration: STOLT	6000 m/s STOLT migration
Migration: TREMOVE	Remove trace padding
FDFILT	BP 40-45-275-300 Hz
Write .hdf5 file	"07b_mig_6000CVS_40-45-275-300_aliasFIX_mg6000.stack"

Table 3.5 Process list of 13_export_segy.job

Process	Details
Read .hdf5 file	"07b_mig_6000CVS_40-45-275-300_aliasFIX_mg6000.stack"
TDCONV1	6000 m/s constant T-D conversion with 20 km final depth
AGC	1000ms for balance after conversion
ADDHDR	Add KKJ3 coordinates into headers at bytes 73 (X) and 77 (Y)
Write SEGY file	"13a_KOSE_final_CVS6000_mg_td6000_BP40-45-275-300.segy"

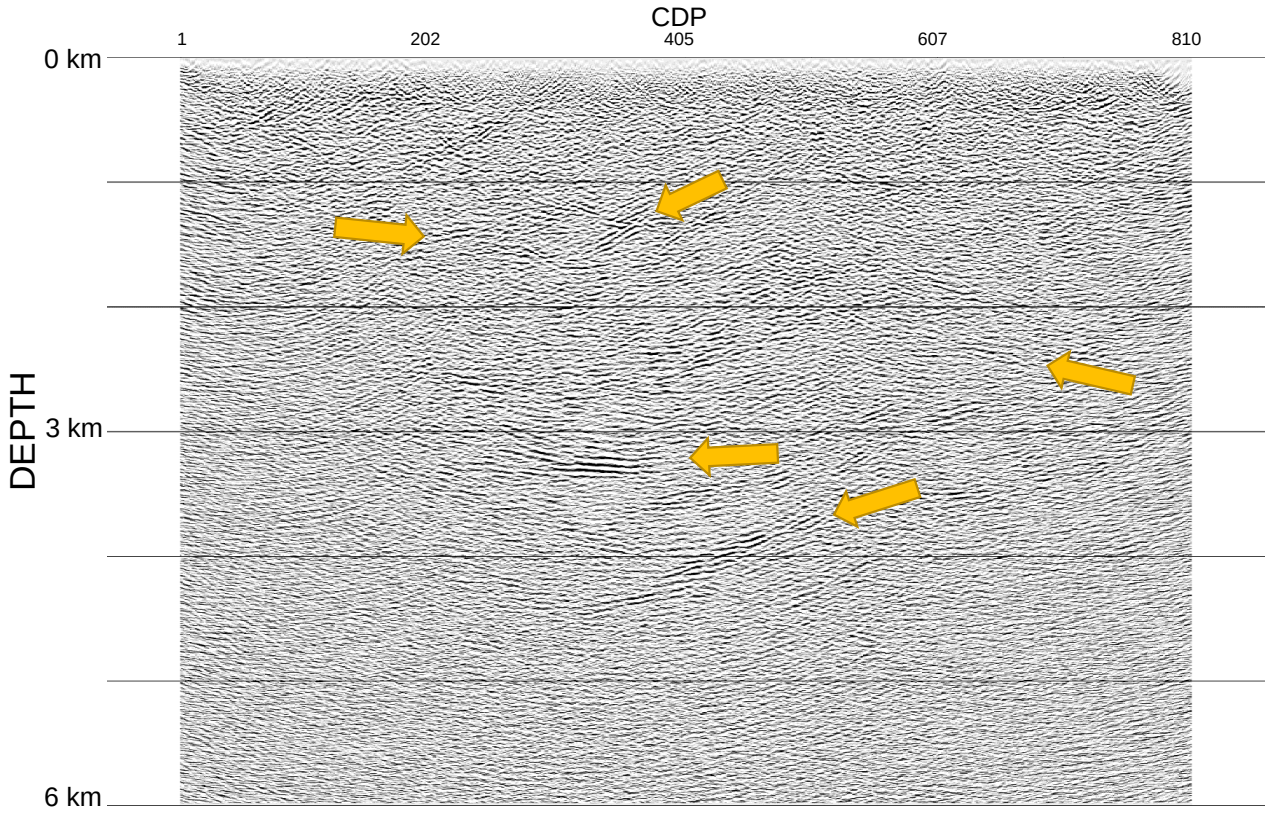

Figure 3.10 The full stack with migration after the processing flow from Table 3.4. Time-depth conversion from Table 3.5 is included.

Pre-stack time-migration (PSTM) was also tested in job flows 10a, 10b and 10c. The processing flow is shown in Table 3.6, below. For the preparation file (job 10a), the data resulting from Table 3.2 were top muted and agc applied, before the Kirchoff pre-stack time-migration algorithm was applied (job 10b). The parameters shown in the table below of the Kirchoff migration were selected after some testing and were shown to return the best results. After the migration, the data were stacked using similar processes as the normal stacking from Table 3.3.

Figure 3.7 shows the result of the PSTM process from Table 3.6 and the segy export job from Table 3.5. The results are very similar to the STOLT migration results, but show somewhat less noise and is thus preferable final stack.

Table 3.6 Process list of 10a_pstm_prepare, 10b_pstm_run and 10c_pstm_stack jobs.

Process	Details
10a_pstm_prepare.job	
Read .hdf5 file	"04a_prestack_proc_aliasFIX_fxdecon_BP40-45-275-300.shots"
SMUTE	Refraction top mute with: ref_mute.smu
AGC	200 ms
Write .csegy file	"10a_pstmPrep_aliasFIX_40-45-275-300_FrontMute.csegy"
10b_pstm_run.job	
IMAGE_K2T	Input: "10a_pstmPrep_aliasFIX_40-45-275-300_FrontMute.csegy" Offset: 40:1000/40 Range: 1000; Protect: 100; Angle: 85; Stretch: 110; Anti-Alias: 2.0 Output: "10b_pstm_aliasFIX_40-45-275-300_6000CVS_r1000.shots"
10c_pstm_stack.job	
Read .hdf5 file	"10b_pstm_aliasFIX_40-45-275-300_6000CVS_r1000.shots"
AGC	200 ms
FDFILT	BP 40-45-275-300 Hz
RUNMIX	Weighted mix of 3 adjacent traces.
STACK	SQRT Normalized stack.
BALANCE	Full trace balance
Write .hdf5 file	"10c_pstm_r1000_40-45-275-300_aliasFIX_6000CVS_mg6000.stack"

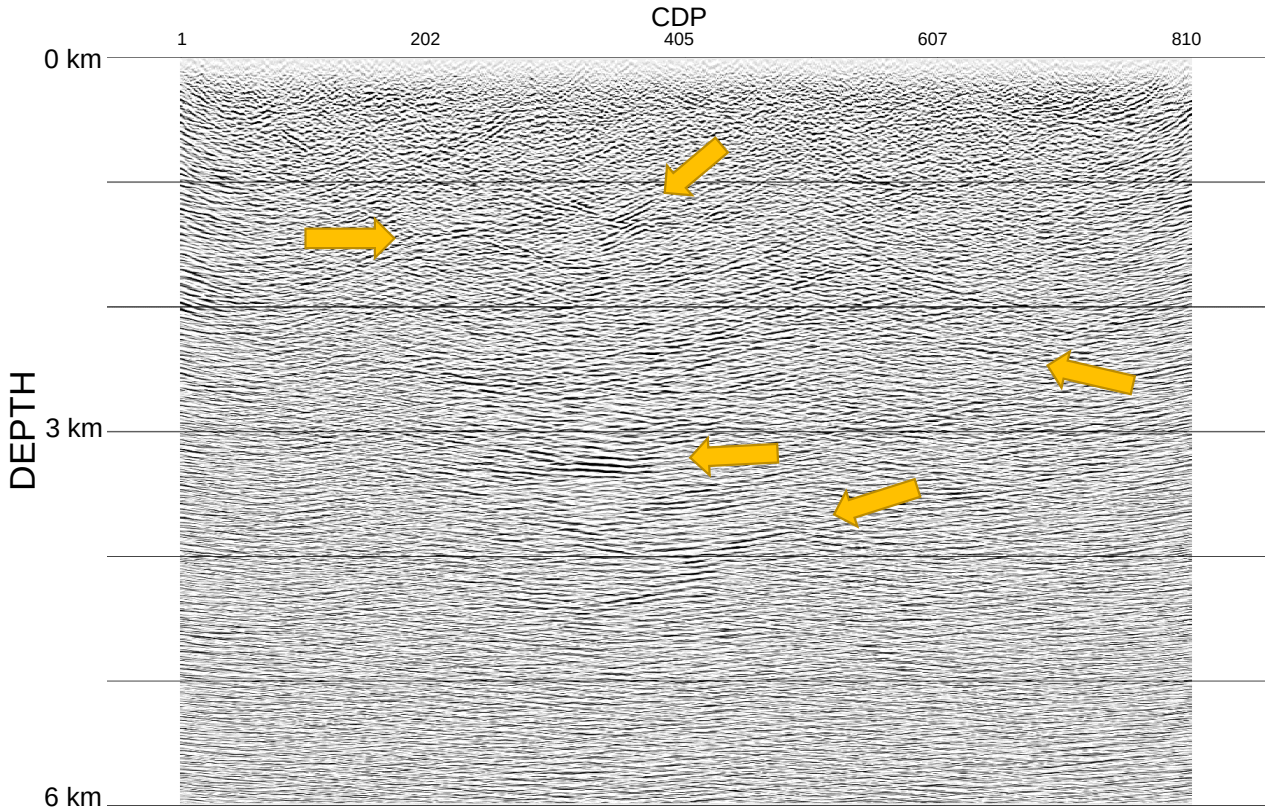

Figure 3.11 The PSTM stack after the processing flow from Table 3.6. Time-depth conversion from Table 3.5 is included.

The top arrow in Figure 3.11 and 3.10 indicates a reflector that has a strange shape. After migration, there should not be “sharp corners” on the reflectors. This could be the result of too low velocity and thus a higher velocity had to be tested. We tested 8000 m/s instead of the usual 6000 m/s. Although it is not a realistic velocity, the dipping of the reflector causes it to have a higher apparent velocity and is thus justifiable. Figure 3.12 shows the same PSTM stack as Figure 3.11 but using 8000 m/s migration and stacking velocity. Here, the reflector is flattened and seems more reasonable and can hopefully aid the modelling.

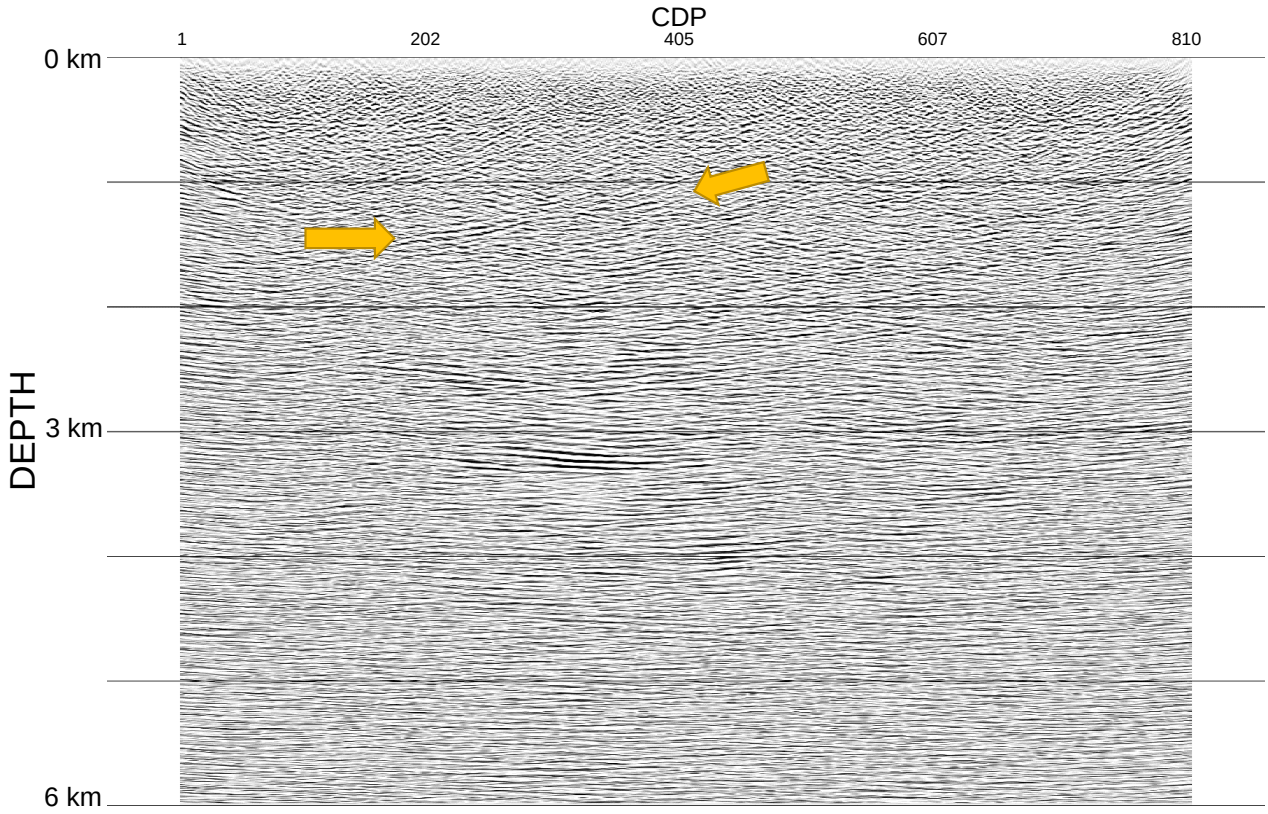

Figure 3.12 The PSTM stack after the processing flow from Table 3.6 but using 8000 m/s migration and stacking velocity. Time-depth conversion from Table 3.5 is included.

4 INTERPRETATION

As it is typical for hardrock seismic surveys, the surveyed seismic reflection profile does not show continuous horizons that would be simple to interpret and correlate with surface geology (Figures 4.1 and 4.2). However, there are wealth of reflectors in the stacked and migrated data. The migration velocity can have minor effect on the dip, depth and subsurface position of the reflections, but will not change the overall reflectivity pattern.

The upper part of the seismic reflection profile has several fairly steeply dipping reflectors that are likely originating from the numerous dolerite dykes in the survey area. These reflectors have dips varying between 25-35° NE along the seismic profile. In the NE end of the profile, an event with 35° SW coincides likely a discontinuous dyke swarm oriented in approximately NW direction.

The most prominent reflections in the KOSE seismic profiles are probably caused by the mafic-(ultramafic) body within migmatitic tonalite that are also source of the strong positive

gravity anomaly of the region. The gravity data models indicate a depth of 1 km for the upper contact of the body. The seismic data show similar depth, but a more complex form of the body.

The most prominent reflector in the seismic profile is at 3300 m depth at CDP 280-320. This is likely originating from the bottom of the mafic body. The strength of reflection is attributed to the contrast in acoustic impedances of the rocks in contact with each other. Also geometry of the reflector can have effect on the amplitude as for example, bowl shaped synclines tend to focus the energy of the seismic waves to image the (subhorizontal) hinge of the fold more clearly than steep limbs. If it is assumed that the Koillismaa mafic-ultramafic intrusion blocks are surrounded uniformly by the migmatitic tonalite in depth, the stronger reflectivity of lower contact compared to the upper contact might suggest that the mafic-ultramafic body is layered. Denser rockmass in the lower part of the body has higher acoustic impedance compared to the upper part, and thus more seismic energy reflects from the contact with migmatitic tonalite.

At CDP 380-420 and depth of 1500 m, there is a reflector that seems to be cut and displaced by other reflector. It is possible that this is a result of too low migration velocity. Higher migration velocity would move the reflectors updip and make them steeper. However, these crossing reflectors can also be interpreted as displacements of lithological contacts caused by faulting. In KOSE case this would mean that the narrow mafic dykes are older than the more extensive mafic-ultramafic body, and faulting has occurred simultaneously with the body.

The gravity models of the mafic-ultramafic body are the results of inverse modelling (fitting data to model), while the seismic data give a more accurate image of the subsurface layering and with higher resolution. The seismic data interpretation concludes that the body reaches the surface in the SW end, which deviates it from the gravity data interpretation. These discrepancies, indicate a more complex body than previously thought. For a more complete geological cross section, all known geology, gravity, magnetic and seismic data should be carefully integrated together.

There are currently no drill holes that would aid the interpretation of the seismic reflection data. In order to evaluate the reliability of the interpretation, it would be advisable to drill two drill holes along the seismic profile. A 500 m long drill hole in the SW end of the profile, at CDP 700, would be suitable to test the continuity of the mafic body closer to the surface. Another longer drill hole at CDP 400-500, up to 1500 m length, with approx. 40° angle towards SW (perpendicular to the strike of the reflectors) would shed light to the interpretation of the shallow dipping events as well as test if the interpretation of the upper contact of the body is accurate (Figure 4.1).

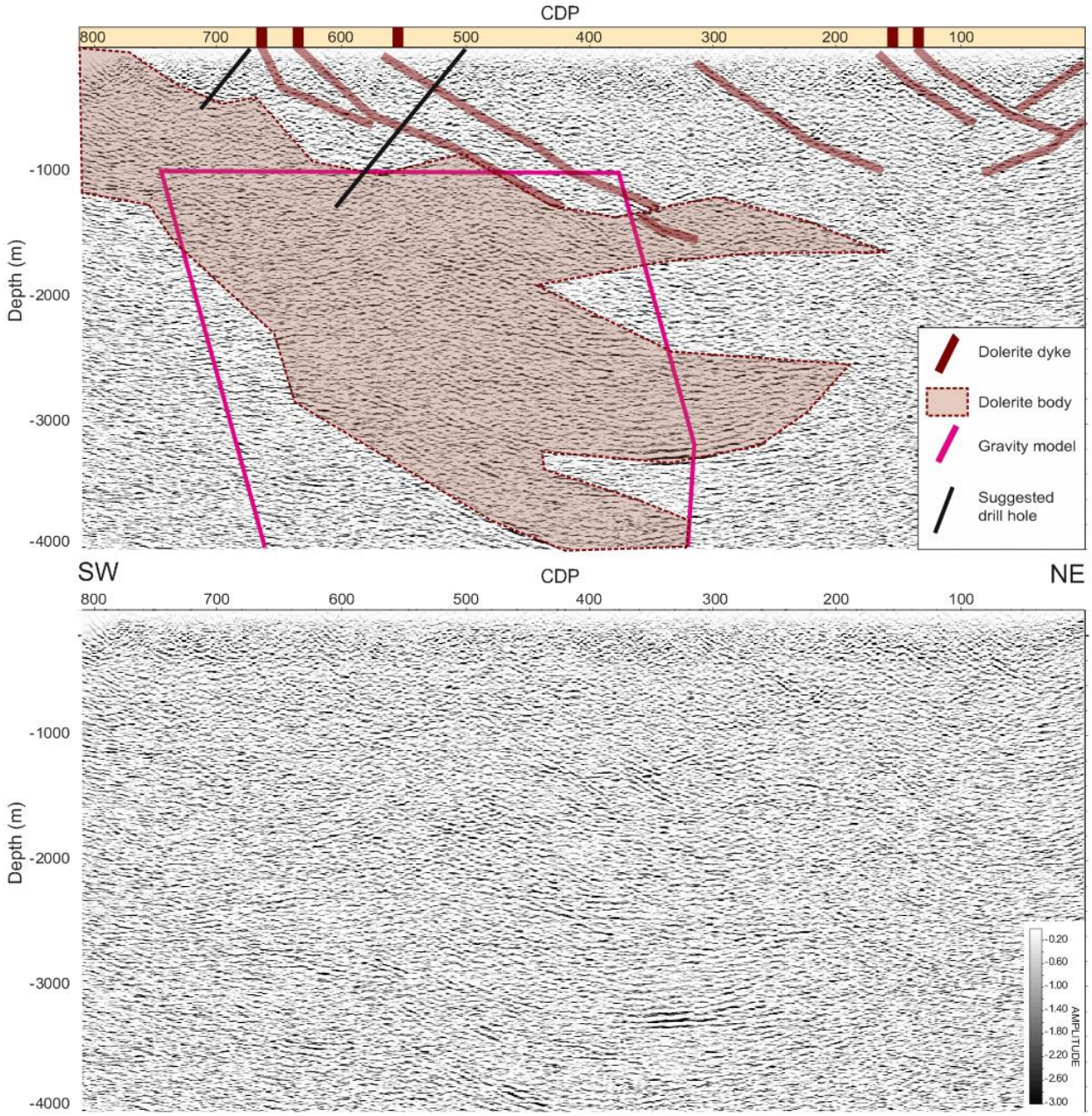

Figure 4.1 One possible interpretation of the Koillismaa seismic reflection profile. The intersection of the gravity model and seismic section is indicated with the pink line. Seismic reflectivity indicates an undulating upper and lower contacts of the mafic body to the hosting migmatitic tonalite. Reflectivity of the upper 1 km can be attributed to the various dolerite dykes of the area. Interpretation of the profile is not straight forward due to lack if continuous prominent reflectors, and interpretation should be considered as one possible model of the subsurface that needs to be tested with drilling. Geological column on top of the seismic section is based on DigiKp (Figure 4.2).

Besides drilling, additional geophysical surveys could shed more light into the geological interpretation of the Koillismaa area. The terrain of the area is not easily accessible for further seismic surveys, if not conducted during winter months when swampy areas are frozen. Audio-Magneto Telluric (AMT) measurements for mapping the conductive structures along the profile could further support the interpretation of the seismic data. It would be advisable to test by drilling to a few shallow reflectors and conduct petrophysical measurements from the drill cores prior to designing new geophysical surveys. Petrophysical measurements are needed to confirm that the geological features of interest actually have detectable geophysical response, and to constrain the interpretation of the geophysical data.

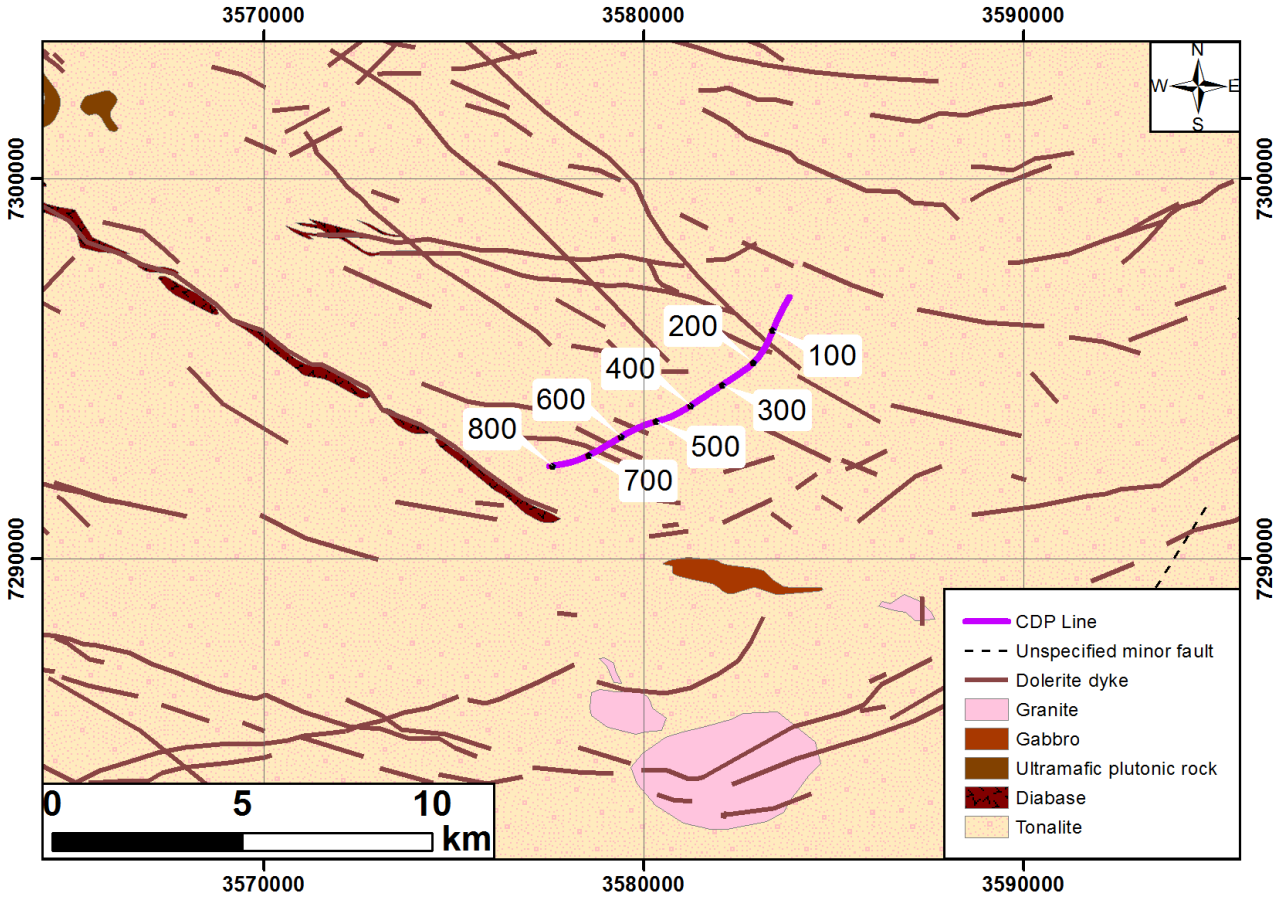

Figure 4.2 A geological map of the area with the CDP of the seismic profile indicated. The map is in KKJ3 coordinates.

5 CONCLUSION

The cooperation between GTK and OU within KoSe project was successful and encourages future collaboration. As usual for hardrock seismic, the data are noisy and challenging to process. In the KOSE survey, 20 m receiver spacing and 40 m source spacing was used, which provides an insight into the major reflectivity in the survey area. The final, processed seismic data show a good number of reflectors enabling interpretation. In this report the survey acquisition and data processing procedures are described in details and first insights and interpretations are made. If considered, interpretation can be further improved in the future e.g. by new surveys or by refining processing.

The upper 1 km of the final seismic section shows several dipping reflectors that are interpreted as a part of a dolerite dyke swarm in the survey area. Most of these reflectors are dipping 25-35° NE along the seismic profile, but few dip 35° SW along the profile. The most prominent reflector in the seismic section is at 3.3 km depth at CDP 280-320 and is interpreted to originate from the bottom of the mafic-ultramafic body. Previous gravity models (Salmirinne & Iljina, 2003), suggest a 1 km depth to the upper body contact, and the seismic data show similar depth, but with a more complex form. Assuming a homogeneous surrounding of the body, the difference between the reflection amplitude of the top and bottom of the body suggest a layered igneous body.

As there are no drill holes in the area to aid interpretation, two drill holes are suggested to be drilled. A 500 m deep drill hole in the SW end of the profile at CDP 700 to test the continuity of the mafic body close to the surface. Another, 1500m long drill hole at CDP 500 with a 40° angle towards SW, would assess the interpretation of the location of the top of the body. Audio-Magneto Telluric (AMT) measurements along the seismic profile could further support the geological interpretation.

6 REFERENCES

Alapieti, T., 2005. Early Palaeoproterozoic (2.5−2.4 Ga) Tornio–Näränkävaara Layered Intrusion Belt and Related Chrome and Platinum-group Element Mineralization, Northern Finland. In: Alapieti, T.T. & Kärki, A.J. (eds.) Early Palaeoproterozoic (2.5−2.4) Tornio–Näränkävaara Layered Intrusion Belt and Related Chrome and Platinum-Group Element Mineralization, Northern Finland. Geological Survey of Finland Guide 51a, 5−11.

Alapieti, T. & Lahtinen, J. J. 2002. Platinum-Group Element Mineralization in Layered Intrusions of Northern Finland and the Kola Peninsula, Russia. In: Cabri, L.J. (ed.), The Geology, Geochemistry, Mineralogy and Mineral Beneficiation of Platinum-Group Elements. The Canadian Institute of Mining, Metallurgy and Petroleum Special Volume 54, 507−546

Iljina, M. & Hanski, E. 2005. Layered mafic intrusions of the Tornio–Näränkävaara belt. In: Lehtinen, M., Nurmi, P.A. & Rämö, O.T. (eds.) Precambrian Geology of Finland – Key to the Evolution of the Fennoscandian Shield. Elsevier B.V., Amsterdam, 101–138.

Iljina, M., Maier, W.D. and Karinen, T., 2015. PGE-(Cu-Ni) Deposits of the Tornio-Näränkävaara Belt of Intrusions (Portimo, Penikat, and Koillismaa) *in* Maier, D., Lahtinen, R., O'Brien, H.:Mineral Deposits of Finland, Elsevier, p. 133-164

Karinen, T., 2010. The Koillismaa Intrusion, northeastern Finland – Evidence for PGE reef forming processes in the layered series. Geological Survey of Finland, Bulletin 404, 176 p.

Salmirinne & Iljina 2003. Koillismaan kerrosintruusiokompleksin tulokanavamuodostuman painovoimatulkinta ja alueen malmimahdollisuudet (osa 1). Geologian tutkimuskeskus. Archive report Q21/2003/1, 20 p, 5 appendices.

APPENDIX A

GLOBE CLARITAS .JOB DESCRIPTIONS

00

- *importSEGD_wGEOM.job:* Import all original SEGD files with headers and convert to SEGY (Table 3.1)
  Outputs:
  - KoSe_VerticalCompData_Full_wGEOM.csgy
  - **KoSe_VerticalCompData_Full_wGEOM.hdf5**

01

- *01_brute_stack.job:* Initial brute stack with HIRE velocities and 6000 CVS.
  Outputs:
  - 01_brute.stack and 01_brute_CVS6000.stack (Figure 3.1)

02

- *02a_QC_refstat_shots.job:* Quality Control of the refraction statics
- *02b_QC_refstat_stack.job:* Quality Control of the refraction statics effects on stack.
- *02c_QC_refstat_writeStack.job:* Write out the brute stack with refraction statics.

03

- *03a_QC_noise.job:* Preparation with SPHDIV and FDFILT for NOISE_QC module.
- *03b_QC_noise_writeShots.job:* Write shots with noise QC applied
- *03c_QC_noise_writeStack.job:* Write stacks from previous job (03b).

04

- *04a_fk_aliasing_fix.job:* Main pre-stack processing job (Table 3.2).
  Outputs:
  - **04a_prestack_proc_aliasFIX_fxdecon_BP40-45-275-300.shots**
- *04b_fk_aliasing_stack_jcs.job:* Anti-aliasing test job for setting various parameters.

05

- *05_mute_analysis.job*: Creation of refraction mute.

06

- *06_jsc_velocity_CVS.job*: Creating Constant Velocity Stacks (CVS) for updating velocity model. However, because of few reflectors, a 6000 m/s CVS was chosen.

07

- *07a_stack_nmo.job:* Stacking of data from 04a (Table 3.3)
  Outputs:
  - **07a_6000CVS_40-45-275-300_aliasFIX.stack** (Figure 3.9)
- *07b_migrate_stacks.job:* Migration of stacked data from 07a (Table 3.4)
  Outputs:
  - **07b_mig_6000CVS_40-45-275-300_aliasFIX_mg6000.stack**

08

- *08a_spstat_prepare.job:* Prepare for residual statics module.
- *08b_spstat_run.job:* Run residual statics module.
- *08c_spstat_QC.job:* QC stacks with residual statics. Decided not to include them as the results worsened.

10

- *10a_pstm_prepare.job:* Prepare data to run PSTM algorithm
- *10b_pstm_run.job:* Run PSTM algorithm.
- *10c_pstm_stack.job:* Stack data from 10b. All is shown in (Table 3.6)
  Outputs:
  - **10c_pstm_r1000_40-45-275-300_aliasFIX_6000CVS_mg6000.stack**
  - **10c_pstm_r1000_40-45-275-300_aliasFIX_8000CVS_mg8000.stack**

12

- *12_makePlotReport_jcs.job:* Make the plots for this report (See .tiff files in Figures/Seismic).

13

- *13_export_segy.job:* Time to Depth conversion, correcting from floating datum to Seismic Reference Datum and adding headers (Table 3.5). These are the final products of the processing
  Outputs:
  - **13a_KOSE_final_CVS6000_mg_td6000_BP40-45-275-300.segy** (Figure 3.10)
  - **13b_KOSE_final_CVS6000_pstm_td6000_BP40-45-275-300.segy** (Figure 3.11)
  - **13b_KOSE_final_CVS8000_pstm_td6000_BP40-45-275-300.segy** (Figure 3.12)

APPENDIX B

Magnetic anomalies on Kenttärata road:

- **Kenttarata anomaliat 27032018_v2.pdf**

APPENDIX C

A1 size, printable seismic sections:

- **Final_Seismic_40-45-275-300_Color.pdf**
- **Final_Seismic_40-45-275-300_Grayscale.pdf**

From *13b_KOSE_final_CVS6000_pstm_td6000_BP40-45-275-300.segy*

APPENDIX D

As mentioned in the Processing section, and Figure 3.6, we also tested a cutoff frequency of 135 Hz, which would effectively eliminate aliasing. Although, the higher frequencies give a crisper image, this lower frequency seismic section shows higher amplitudes than in the other seismic sections. This can be convenient, when in doubt of interpretation. The processing sequence is exactly the same as before, but in Table 3.2, the *Anti-Alias* section is removed and the first *FDFILT* is changed from 40-45-275-300 Hz to 40-45-120-135 Hz. As in Appendix A, the output files are:

- **04a_prestack_proc_fxdecon_BP40-45-120-135.shots** (Figure 3.6a)
- **10c_pstm_r1000_40-45-120-135 _6000CVS_mg6000.stack**
- **13b_KOSE_final_CVS6000_pstm_td6000_noAliasFix_BP40-45-120.segy**

A1 size, printable seismic sections:

- **Extra_Seismic_40-45-120-135_Color.pdf**
- **Extra_Seismic_40-45-120-135_Grayscale.pdf**

From *13b_KOSE_final_CVS6000_pstm_td6000_noAliasFix_BP40-45-120-135.segy*